Multitone Measurements for the Characterization of EMI Filters at High Power Levels

José M. Aponte Urmeneta
Power Electronics & Electromagnetic Compatibility Group
University of Twente
Enschede, The Netherlands
j.m.aponteurmeneta@student.utwente.nl

Committee members:
Dr. Ir. N. Moonen
MSc. D. Nemashkalo
MSc. P. Koch
Dr. Z. Mahfouz

***Abstract*—This paper outlines the development of an Electromagnetic Interference (EMI) filter measurement system that allows the analysis of Non-Linear Time Invariant (NLTI) and (Non-)Linear Time Variant (NLTV) behavior. CISPR 17 is one of the common standards for the characterization of EMI filters. CISPR 17 provides the guidelines to measure the performance of filters with small signals and a 50/50 Ω source/load configuration as well as an approximate worst case scenario. The performance of EMI filters is evaluated with the Insertion Loss (IL) curves. Such measurement is not representative of in-situ performance of the filter, as it does not evaluate filters under in-situ conditions which may display NLTV effects. During this study, high power levels are used when evaluating an EMI filter to approximate in-situ behavior. The filter components may change characteristics over time due to wear, temperature, and non-linear effects like saturation. These changes manifest in a change in filter performance, observable through the IL curves, which can be considered NLTV behavior. Non-linear behavior due to the high voltage applied was observed, in addition to LTV behavior after increasing the filter's temperature.**

***Index Terms*—Insertion Loss, Linear Time Variance, Multitone, Non-Linear Time Invariance, Non-Linear Time Variance.**

I. Introduction

Electromagnetic Interference (EMI) poses a significant challenge in power electronic systems characterized by fast transient behaviors, such as those employing switched power devices and converters [1]. Passive EMI filters serve as an indispensable solution to mitigate the adverse effects of EMI on the integrity of power lines [1], emissions due to high clock speeds [2], and susceptibility to noise caused by RF signals [3].

Insertion Loss (IL) is a crucial metric in evaluating EMI filter performance. Conventionally, the analysis is done in the frequency domain [4]. Currently, characterizing EMI filters involves employing distinct setups to measure Common Mode (CM) IL, Differential Mode (DM) IL, and Normal Mode (NM) IL, as per the CISPR 17 standard. The standard measurement is done with a small signal and a 50/50 Ω source/load terminating impedance [5]. Additionally, a worst case approximation measurement with 0.1/100 Ω termination [4], which allows the evaluation of the filter under a more realistic condition is seldom done. However, this method is time-consuming due to the number of measurement setups required, a limited frequency range caused by the need for baluns, and the frequency domain analysis [6].

Weight-critical applications such as aerospace demand stringent adherence to specific limits to maintain the integrity and transient behavior of electrical systems. Standards like MIL-STD-704F and RTCA-DO-160 outline specific criteria for ensuring the integrity of aircraft power systems, particularly concerning conducted EMI, which can jeopardize bus voltage quality [7]. In scenarios where electrical loads average 40 kW during flight [7], compliance with standards such as MIL-STD-461g, which specifies limits for conducted emissions in power leads, is paramount.

Factors such as fast transients and CM voltage levels, among others, influence the saturation of the magnetic core in a Common Mode Choke (CMC) [8]. Over-designing the magnetic core is a safe way to prevent saturation [9], however this is not desirable in the aerospace industry since weight restrictions are strict. Fast transients, in combination with high power levels, may lead to an increase in the components' surface temperature [10], which may affect the filter's performance. Awareness of this behavior, which can be considered Linear Time Variant (LTV), may allow the design of a filter robust to such effects.

A study [6] proposed an alternative method to measure the IL of a filter involving the Continuous Wave Frequency Sweep (CWFS) method across relevant frequencies. It eliminated the need for baluns to evaluate the DM IL, and the CM IL evaluation can be done with the same setup, improving the versatility of the setup and reducing evaluation time. However, this setup still uses small signal excitations for the analysis of EMI filters and it does not allow (Non-)Linear Time Variant (NLTV) behavior investigations.

As an extension to the work in [6], this paper proposes the use of a high-power trapezoidal signal in a similar setup to stress test filters and assess their performance under operating limits. By employing time-domain multitone, multichannel measurements, the study seeks to overcome drawbacks associated with conventional frequency-domain measurements [6], offering a more time-efficient and comprehensive evaluation method which allows the exploration of NLTV behavior of the EMI filter. The proposed approach aims to streamline this process by consolidating multiple measurements into a

single setup, which allows the investigation of NLTV behavior thereby saving time and enhancing optimization and automation prospects.

This paper describes the measurement setup for EMI filter performance evaluation, which uses a high-power signal in a multitone excitation. Section II describes the current measurement methods, as well as the drawbacks and limitations of such methods. Additionally, the required mathematical analysis for the post-processing of the measurement data is explained. Section III outlines the importance of evaluating NLTV behavior. Furthermore, the power levels present in the relevant application are discussed. Section IV describes the hardware used, presents the simulation of the setup, and outlines the characteristics of the physical design. Finally, the measurement procedure is described and the gathered results are processed and presented in Section V, which after analysis, are discussed and concluded upon in Section VI.

II. Theoretical Background

A. State of the Art

CISPR 17 evaluates EMI filters in the range of a 10 kHz to 10 GHz [4]. This method evaluates different types of filters. For instance, power line filters are conventionally evaluated in the 10 kHz to 30 MHz range [5]. The IL is determined based on the ratio between the applied signal's magnitude without the filter and with the signal's magnitude after being attenuated with the filter present [11]. This is defined by (1).

$$\mathrm{IL} = 20\log\left(\frac{V_{\mathrm{L}\omega_0}}{V_{\mathrm{L}\omega}}\right) \tag{1}$$

Where $V_{\mathrm{L}\omega_0}$ denotes the magnitude of the unfiltered signal and $V_{\mathrm{L}\omega}$ denotes the magnitude of the filtered signal.

CISPR 17 measures the IL based on a small signal excitation in a standard 50/50 Ω source/load termination. Additionally, CISPR 17 includes an approximate worst case scenario at 0.1/100 Ω [5]. However, this IL measurement is not representative of the in-situ behavior of the filter [6]. Furthermore, the CISPR 17 method does not allow the exploration of in-situ LTV behavior.

As discussed in [6], the characterization of an EMI filter requires up to 24 different measurements in addition to three different measurement setups. The CM measurement setup differs from the DM setup in one essential way - it does not require balun transformers. The baluns themselves limit the measurement frequency range. To overcome the different measurement setups, an alternative dual-source and dual-load setup was analysed and evaluated, and [6] concluded it is possible to determine the IL of a filter with a single setup consisting of one Arbitrary Waveform Generator (AWG) with two Phase-Lock Looped (PLL) output channels. The aforementioned setup is shown in Fig. 1.

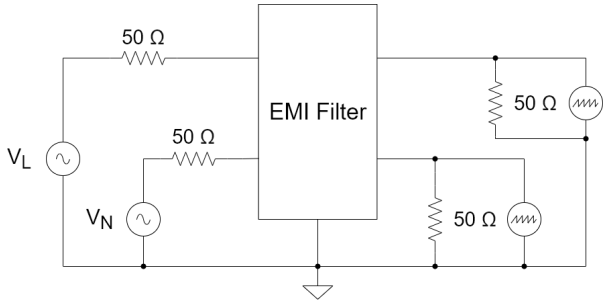

Fig. 1: Dual channel measurement setup.

The setup must determine both the CM IL and the DM IL, thus one source is connected to each of the filter's terminals. As shown in [6], the input signals must be combined to obtain the CM and DM components. The CM component is obtained with (2) and the DM component is obtained with (3) [6].

$$V_{\mathrm{CM}} = V_{\mathrm{L}} + V_{\mathrm{N}} \tag{2}$$

$$V_{\mathrm{DM}} = V_{\mathrm{L}} - V_{\mathrm{N}} \tag{3}$$

Assuming the applied input signals are sinusoidal excitations with the same frequency, the input voltages V_{L} and V_{N} are given by (4) and (5) [6].

$$V_{\mathrm{L}} = A\sin\left(\omega t + \varphi_1\right) \tag{4}$$

$$V_{\mathrm{N}} = A\sin\left(\omega t + \varphi_2\right) \tag{5}$$

From (4) and (5), it can be inferred that to obtain the CM component, the input signals must be in-phase, and to obtain the DM component, the signals must be 180° out-of-phase [6].

Since summation is a linear operation, it can be assumed that a sum of sinusoids with different frequencies will undergo the same analysis as a single sinusoid with a specific frequency. If V_{L} and V_{N} are sums of sinusoids of different amplitudes and frequencies, then applying (2) and (3) will result in (6) and (7).

$$V_{\mathrm{CM}} = \sum_{n=0}^{N} 2A_n \sin\left(\omega_n t + \frac{\varphi_1 + \varphi_2}{2}\right)\cos\left(\frac{\varphi_1 - \varphi_2}{2}\right) \tag{6}$$

$$V_{\mathrm{DM}} = \sum_{n=0}^{N} 2A_n \cos\left(\omega_n t + \frac{\varphi_1 + \varphi_2}{2}\right)\sin\left(\frac{\varphi_1 - \varphi_2}{2}\right) \tag{7}$$

B. Proposed Method

As mentioned previously, the evaluation of the IL of an EMI filter is done in the frequency domain and is time-consuming. The IL measurement of a filter based on the CWFS method is limited by the fact that every point taken must be measured with a single frequency.

A multitone analysis for the measurement of a device's impedance has been demonstrated to work effectively in [12]. Instead of sweeping through individual frequencies, a chirp signal containing frequencies between 30 Hz and 100 kHz was used to characterize the impedance.

A multitone approach requires analysis through a Fast Fourier Transform (FFT). The chirp signal used in [12], which contains multiple frequency components, effectively reconstructed the impedance curve within the range of 30 Hz and 100 kHz. The multitone signal concept is extended to a different time-domain signal as well as a different purpose, namely the IL measurement of an EMI filter.

In this paper, a trapezoidal signal is chosen for its ease of implementation with high power levels. It contains a predictable spectrum and the set of harmonics that can be used for the IL measurement consists of the odd multiples of the fundamental frequency of the trapezoidal signal. Mathematically, the odd harmonics are the only harmonics present in such a signal [11]. Noise and other distortion sources will cause an increase in the even harmonics' magnitudes, but these harmonics will be ignored during the IL calculations since they are not mathematically relevant [11].

The spectrum of a trapezoid is determined by the on-time of the signal, as well as by the rise and fall times [11]. The spectrum is limited mainly by the rise and fall times of the signal [13]. According to Fig. 2, the relation between the rise time and the second pole on the frequency axis limits the amplitude of the harmonics by the -40 dB per decade envelope. A faster rise time increases the measurement bandwidth and the number of harmonics that can be used for the accurate IL plot reconstruction.

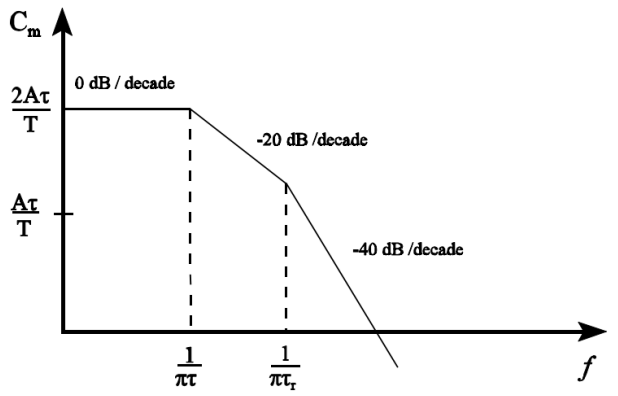

Fig. 2: Envelope of the spectrum of a trapezoidal signal with poles defined by the signal's on-time τ and rise time τ_r [11].

Using the CWFS method, if the frequency resolution chosen to reconstruct the IL curve is 10 kHz, then a total of 3000 measurement points are needed for the range between 10 kHz and 30 MHz. Conversely, with the proposed multitone method, and using a fundamental frequency of 10 kHz, the first 1500 harmonics of the trapezoidal signal cover the entire frequency range in a single measurement. Therefore, the measurement method considered in this paper facilitates the evaluation of an EMI filter under different circumstances, such as high power and temperature changes in a more streamlined manner.

III. Non-linear Time Variant Behavior

Under in-situ operation, an EMI filter may not exhibit the IL measured by the CISPR 17 method. For instance, fast transients may cause the saturation of the magnetic core in a CMC [8]. Saturation flux density in the core is influenced by the CM path resonance and the CM voltage amplitude [9]. Thus, high CM voltages can lead to a change in the filter's behavior due to saturation. This is considered Non-Linear Time Invariant (NLTI) behavior.

Additionally, high current levels in the filter due to the high CM and DM voltages may lead to an increase in temperature in the filter's components. A change in temperature of the dielectric material inside a capacitor results in a capacitance change [14]. This capacitance change affects the IL of the filter and is considered LTV behavior.

A. Power Levels

The relevant power levels present under in-situ performance are evaluated in this subsection. First, CM levels are discussed, followed by the DM levels. The considered voltage and current levels will be used to measure a Commercial Off-the-Shelf (COTS) EMI filter to evaluate it under in-situ performance.

Power converters are present in most applications today. Drives and switching power supplies are common sources of CM noise [1]. The level of CM emissions depends on the type of converter used. In the automotive industry, Electric Vehicles (EV's) require inverter-based drives to power the motors. EV's typically run at high power levels, as well as high frequency - around 100 kW at 20 kHz [15]. The traction drive explored in [15] created CM voltages with a maximum amplitude of 20 V. Another study analyzed the conducted emissions generated in a motor drive system comprised of a battery, an Insulated-Gate Bipolar Transistor (IGBT) driven inverter, and the motor, and found that the CM noise levels were at a peak of 55.37 V [16]. These conducted emission levels are typical in a system handling high power and fast transitions.

Additionally, DM noise, affects the power quality of the dc bus used to supply power to the device [17]. Another study evaluated a Critical Conduction Mode Power Factor Correction (CRM PFC) circuit and their DM noise output. The expected DM current levels that will affect the filter are around 125 dBμA, which correspond to around 1.8 A of differential noise current [18].

IV. Measurement Setup

This section outlines the measurement setup designed for this study. Then, the chosen hardware is presented. The hardware includes the Printed Circuit Board (PCB) designed, the power components chosen, and the switches used. Additionally, the output impedance of the input sources used is modelled. Then the results of the simulated setup are shown. Finally, the physical implementation and measurement equipment used are described and a few key limitations of the setup are discussed.

A. Proposed Setup

The proposed measurement setup is an extension of the concept presented in Fig. 1 [6]. The new setup allows the evaluation of NLTV behavior by injecting high-power trapezoidal signals with levels determined by the voltages and currents mentioned in Section III. Additionally, it allows the evaluation of the approximate worst case scenario (0.1/100 Ω) without requiring a different setup. During this study, only the 50/50 Ω termination case is measured and evaluated to validate its similarity with the CISPR 17 method. The proposed setup is shown in Fig. 3.

In contrast to the setup analyzed in [6], the proposed setup includes high-power tolerant components to allow the injection of high-powered signals into the filter, in addition to switches that allow the selection between the standard 50/50 Ω scenario and the worst case approximation of 0.1/100 Ω.

B. Hardware

1) PCB: The PCB was designed with a six-layer FR4 board with $\varepsilon_r = 4.3$. To consider the measurement trace electrically short for the entire measurement bandwidth of 10 kHz to 30 MHz, the length of the trace was limited to 482 mm, which is one tenth [11] of the wavelength of a 30 MHz signal.

According to [19], the minimum trace width needs to be 0.338 mm to prevent a rise in trace temperature above 10 °C when a current of 1.8 A is flowing through the 70 μm thickness trace. The signal traces were over-dimensioned to support a current of 5 A. Therefore, the minimum width is limited to 1.38 mm. This minimum width suffices in a 4-layer board and its height from the top layer to the bottom layer to achieve a 50 Ω characteristic impedance. However, due to the overlap some traces must have, 6 layers are required to prevent discontinuities in the ground plane under the microstrip traces.

The characteristic impedance of the aforementioned traces is 50 Ω to prevent reflections [11]. For a six layer board, a 70 μm trace thickness, and a height to ground plane of 1.25 mm, the required trace width to obtain a 50 Ω characteristic impedance is 2.3876 mm.

2) Power Components: The source and load impedances must handle 1.8 A as the approximate upper limit because of the power levels mentioned in Section III. The setup was over-dimensioned to support currents of up to 3 A for a short period of time by paralleling impedances.

The chosen power resistors are rated for 100 W and have a 20 nH Equivalent Series Inductance (ESL). The resistors need a heatsink to dissipate the heat generated by the large currents.

The heatsink can create a CM noise path through capacitances to ground [20], which could potentially interfere with the IL measurement. The heatsink may be grounded to prevent high-voltage coupling via the heatsink's capacitance. However, this increases the parasitic capacitance to ground of the heatsink. Leaving the heatsink floating creates a second capacitance in series, which reduces the effective capacitance to ground [20]. Therefore, the heatsink is left floating to reduce the parasitic capacitance, and its value is modelled as 13.85 pF based on the heatsink's geometry.

3) Relay Switches: The switches used are Double Pole Double Throw (DPDT) relays. These are useful for a dual

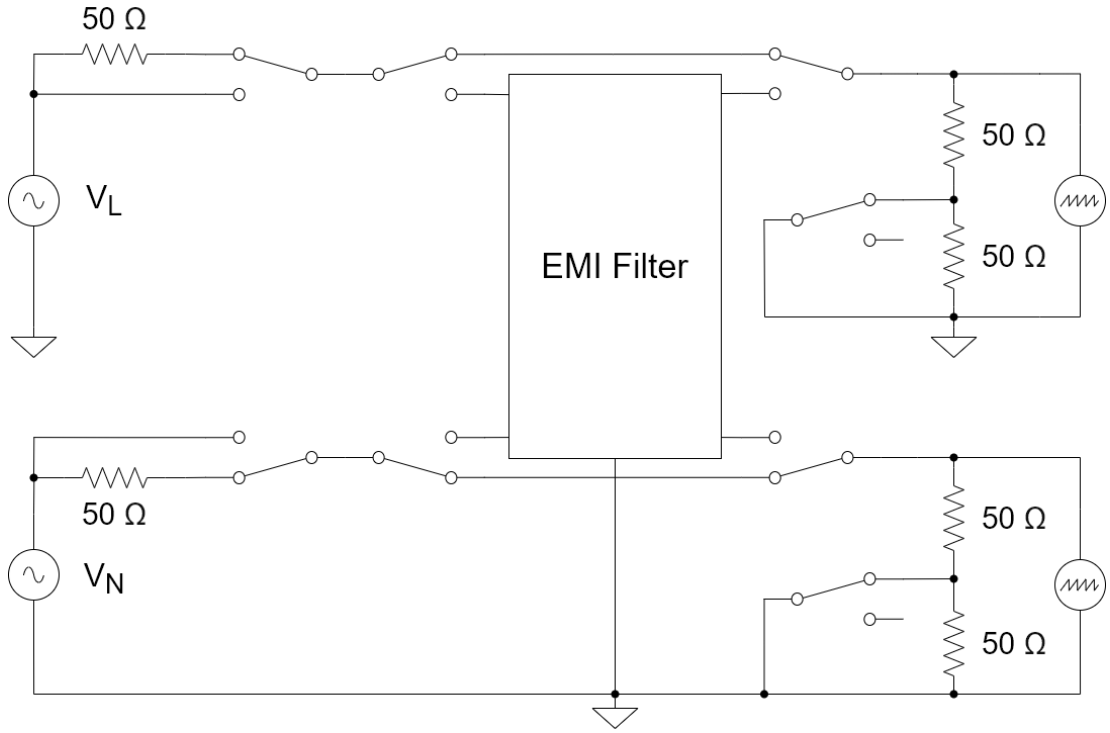

Fig. 3: Proposed measurement setup including switches that allow the selection of unfiltered/filtered measurement and of a scenario.

channel setup because of the dual path switched in tandem. They allow a compact driving circuit because it reduces the amount of relay drivers needed per switch. The relays have parasitic inductances and capacitances. A study [21] investigated the conducted EMI produced by relay contacts. The parasitic values for the components representing the mechanical configuration of a DPDT relay were determined. The relays used in the designed setup are the same DPDT type. These parasitic impedances interrupt the signal's path of the measurement traces with $Z_0 = 50\,\Omega$ and must be accounted for in the simulations. A model of the relay contacts [21] is shown in Appendix A in Fig. 17.

4) Half-Bridge Output Impedance: The provided driving voltage sources for this study are a pair of Silicon Carbide (SiC) transistor evaluation kits. The part numbers are shown in Table I. The transistors are used in a half-bridge configuration. The evaluation kits' manufacturer [22] provides the circuit schematic of the evaluation board. The output impedance was modelled after that schematic and is shown in Fig. 4.

This output impedance (shown as X_9 and X_{10} in Appendix A Fig. 18) can be considered in series with the voltage source and will add to the placed 50 Ω source impedance, thereby noticeably affecting the IL in the MHz range [23].

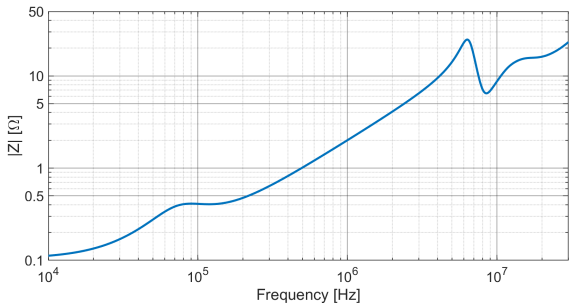

Fig. 4: Half-Bridge SiC transistor evaluation kits' output impedance.

C. Simulations

To determine the effectiveness of the proposed measurement method, the setup was modelled and simulations were run in LTspice. It is worth noting that the maximum time step specified in the simulation settings affects the dynamic range of the frequency analysis. A shorter maximum time step prevents noise in the high-frequency portion of the spectrum. Furthermore, a minimum sampling rate of 1 GSa/s is necessary to achieve a 1 kHz frequency bin resolution in the frequency domain when recording data for 1 ms. The timestep setting is responsible for the noise in the higher frequency portion of the spectrum.

The modelled parts were added to the simulation and the schematic is shown in Appendix A Fig. 18. The signals measured at the 'line' and 'neutral' nodes on Fig. 18 are analyzed in the frequency domain after being combined by (2) and (3). Afterwards, the IL is calculated by using (1) [11]. An AC sweep was run to obtain the expected IL using the CWFS method, and is compared to the multitone simulation result. For the proposed setup's simulation, the time-domain input signal is a trapezoidal wave (see Fig. 5), and both sources are in-phase for the CM measurement and 180° out-of-phase for the DM measurement.

The filter analyzed in this paper is a COTS EMI filter, the schematic of which is shown in Appendix A Fig. 19. A model of the filter is required for the simulations to compare the theoretical data with the measured data. Fig. 6 was obtained after the data processing.

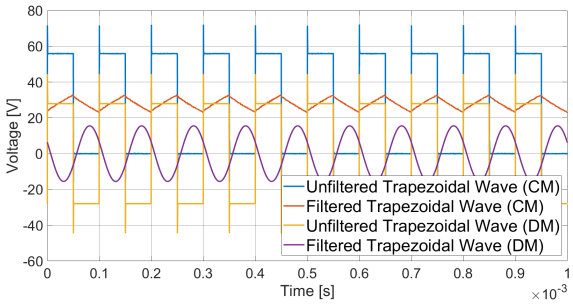

Fig. 5: Simulated time-domain trapezoidal waves with a fundamental frequency of 10 kHz.

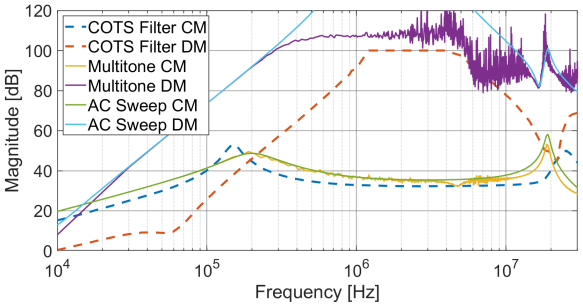

Fig. 6: IL result obtained from the multitone simulation (yellow and purple), in addition to the datasheet-provided IL (blue and red), and the CWFS IL (green and cyan).

The simulation results show that the multitone analysis is able to reconstruct the IL curve of an EMI filter with a reasonable degree of accuracy. The mismatch between the IL of the CWFS method and the IL of the multitone method is due to the additional impedance introduced by the parasitics of the components used in the setup, in addition to the relatively high maximum timestep of 1 ns used for the simulation.

D. Measurement Equipment

TABLE I: Parts list of used equipment.

	Parts	Name	Details
1	Oscilloscope	Keysight DSOX3024A	@4 GS/s (2 GS/s 2 Channel)
2	AWG	Teledyne T3AFG120	@1.2 GS/s
3	2x SiC Evaluation Boards	CRD8FF1217P-1	Half-bridge configuration
4	Power Supply	Tenma 72-2720	
5	High Voltage Power Supply	Kepco Power Supply	ID. 0620
6	PCB	-	Built

The DSOX3024A scope has a sampling rate of 4 GSa/s which is enough to capture two channels simultaneously at 2 GSa/s. Since the minimum sampling rate required is 1 GSa/s as previously mentioned, the available sample rate is sufficient for accurate detection of very high frequency components present in the injected signal.

The practical setup consists of a pair of half-bridges acting as the high-power sources injecting power into the filter. The CRD8FF1217P-1 evaluation boards have an optical and isolated control signal input [22]. Therefore, the 50 Ω output impedance of the AWG does not influence the measurement.

The output voltages are measured with different channels on the oscilloscope. The input signals are generated with the AWG and are applied to the evaluation boards' control signal input pins. The input signals are 180° out-of-phase because [22] specifies the input signals must be inverse of each other. Those input signals drive a single bridge, therefore identical waveforms must be generated to drive the second bridge.

The sources outputs are connected to the built PCB at the IN_1 and IN_2 terminals. The sources and the PCB are connected with short wires to prevent adding additional parasitic inductance into the measurement path.

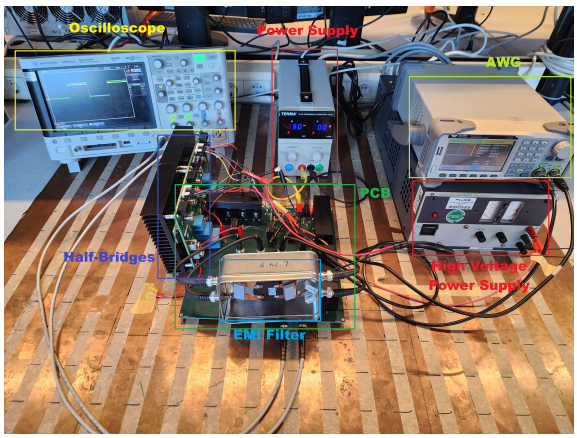

Fig. 7: Measurement setup.

E. Limitations

The most significant limitation for the rise time is the behavior of the MOSFETs. According to [24], the rise time of the MOSFETs is 14 ns, while the fall time is 22 ns. For simplicity, it is assumed that both rise and fall times are equal and limited to 22 ns since such a small difference in rise and fall times does not significally impact the spectrum of the trapezoidal wave [25]. If the rise time cannot be improved beyond 22 ns, the measurement bandwidth will be reduced to about 14.47 MHz as per Fig. 2.

Measuring the signals with high temporal resolution is paramount to prevent distortion and additional noise in the time-domain signals due to the Analog-to-Digital Converter (ADC) in the scope. Increasing the amplitude of the signal can only improve the signal-to-noise ratio (SNR) until the amplitude of the wave reaches the maximum measurable voltage in the scope. If the signal rises above the maximum measurable voltage, the signal will be clipped and this will induce distortions in the post-processing.

Naturally, the dynamic range of the measurement instruments is limited at higher frequencies because of the ADC noise [26], resolution [27], and bit-depth, as well as the internal memory depth to store waveform files. Therefore, together with the higher frequency attenuation due to the rise time, the accurate measurement of the IL at the higher frequency harmonics becomes unfeasible.

V. Results

This section outlines the measurement procedure used for the experiment and presents the measured IL curves. The small signal measurement result is shown first, followed by the large signal result. Afterwards, the observed NLTI behavior is discussed. Finally, the LTV behavior of the EMI filter is displayed.

A. Measurement Procedure

The board was set up in the 50/50 Ω termination configuration. The experiment consisted of two sets of measurements. The first set of measurements taken were done with a small signal to evaluate the similarity to the CISPR 17 method. The second set utilized a large signal to evaluate the filter under approximate in-situ performance. The steps taken are described as follows:

1) The CM and DM IL curves are evaluated at a temperature of 25 °C.
2) The temperature of the EMI filter is increased by applying heat with a hot air gun set to 430 °C.
3) Another measurement is taken when the filter's surface temperature reaches 35 °C.
4) The temperature of the filter is increased until the components' surface temperature reaches 120 °C.
5) A last measurement is taken.

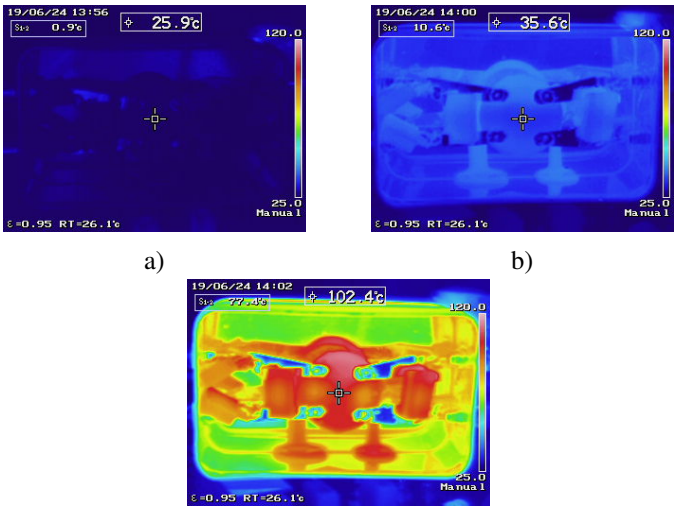

a) b)

c)

Fig. 8: EMI filter at different temperatures. a) 25 °C. b) 35 °C. c) 120 °C.

To reconstruct the IL curve for different temperatures, a single unfiltered measurement is needed since the behavior of the unfiltered measurement is independent form the filter's temperature. The unfiltered measurement serves as the reference by which the filtered waves are compared and evaluated. Thus, every subsequent measurement is done on the filtered trapezoidal wave case.

B. Small Signal Measurement

The first measurements were taken with a 10 kHz small signal trapezoidal wave as an input signal. The time-domain waveforms are shown in Fig. 9.

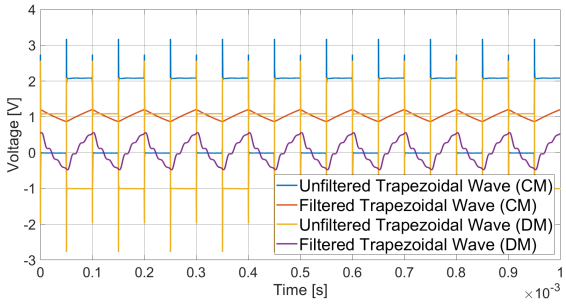

Fig. 9: Applied small signal CM (blue) and DM (yellow) trapezoidal waves compared to their filtered versions.

The measured time-domain signals were subjected to the same post-processing done for the simulations. It can be observed that the CM signal shown in blue in Fig. 9 is filtered similarly to the simulation results (shown in red).

The DM signal attenuation differs from the simulated one because lower frequencies seem to be attenuated less than what the simulation predicts. This effect can be observed in the reconstructed IL curves. The reconstructed IL curves are shown in Fig. 10 and Fig. 11 for CM and DM, respectively.

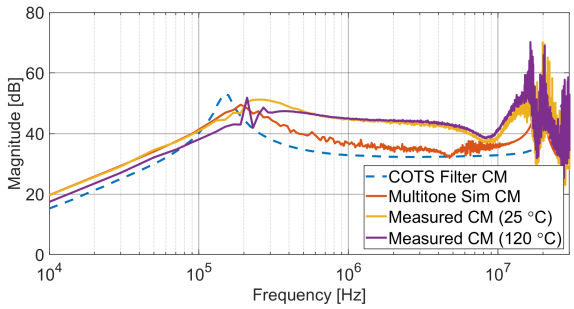

Fig. 10: Effect of a temperature increase on an EMI filter in the CM IL when using a small signal for measurement.

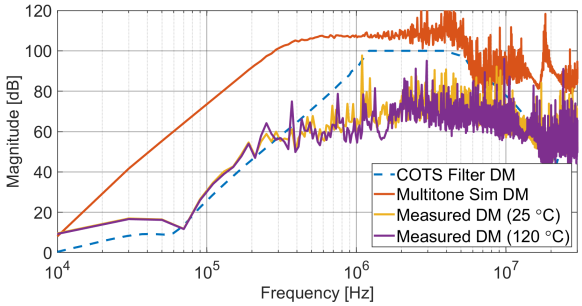

Fig. 11: Effect of a temperature increase of the EMI filter in the DM IL when using a small signal for measurement.

The noise in the high frequency portion of the spectrum is due to the rise time limitation. The magnitude of the harmonics beyond 14.47 MHz is too small to be measured accurately with the equipment used. Furthermore, in Fig. 11 there is an upper limit in the attenuation due to the dynamic range of the oscilloscope used. This limit is around 70 dB.

Despite the limitations in dynamic range, the IL of the measured EMI filter follows the predicted CM curve from 10 kHz to 200 kHz. On the other hand, the DM IL follows the datasheet specified IL more closely than the simulation prediction over the entire frequency range.

C. Large Signal Measurement

The effect of NLTI behavior due to, for instance, the CMC magnetic core saturation can be seen in Fig. 12. Instead of following the predicted filtered CM signal as in the simulations, employing a high-voltage input signal causes the filter to saturate. This saturation prevents the filter from attenuating low frequencies effectively. Thus, the red line on Fig. 12 almost matches the unfiltered wave (blue).

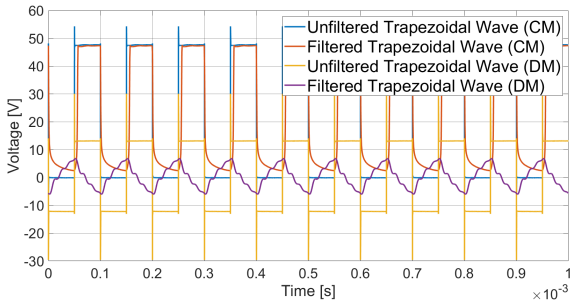

Fig. 12: Measured large signal time-domain waveforms. Unfiltered CM signal (blue), filtered CM signal (red), unfiltered DM signal (yellow), and filtered DM signal (purple).

The signal's rise time does not affect the saturation of the core in the case of a small signal input. The change in inductance over the on-period of the wave happens when the magnitude of the signal applied increases above 12 V.

D. Non-Linear Time Invariant Behavior

The resulting IL curves reconstructed from a large signal applied on the system are shown below. Fig. 13 shows the measured CM IL and Fig. 14 shows the DM IL.

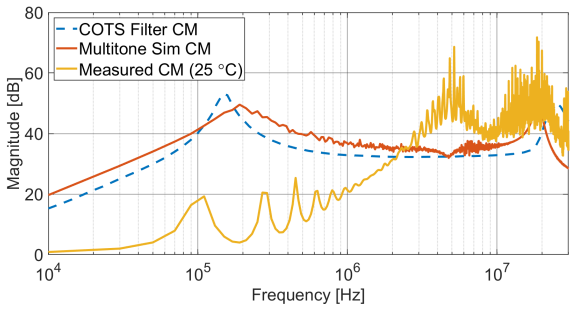

Fig. 13: Non-linear effect of saturation in the CM IL for an EMI filter when using a large signal for measurement.

Already, a difference in IL response can be observed between using a small signal and a large signal to characterize the filter. The high volt-second transient from the rise time can cause the saturation of the CM core [8]. This is reflected in the lower frequency part of the spectrum where there is attenuation under 20 dB until approximately 1 MHz. An interesting artifact of the non-linear effects is the appearance of resonance points and the creation of lobes in the range from 10 kHz to 2 MHz in the CM IL shown in Fig. 13.

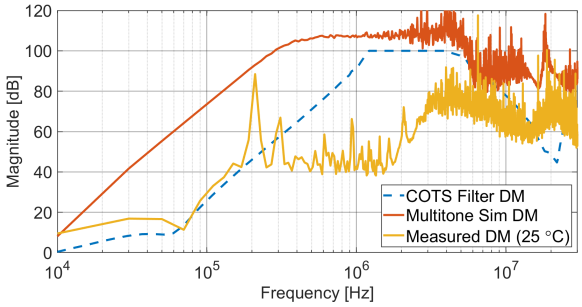

Fig. 14: Effect of saturation due to the high voltage applied in the DM IL for an EMI filter when using a large signal for measurement.

The DM IL is affected only in the range between 200 kHz and 3 MHz when using a large signal to evaluate the filter. Compared to Fig. 11, the IL was reduced by around 20 dB within this frequency range. The effect can be seen in Fig. 14.

E. Linear Time Variant Behavior

An increase in temperature causes a change in the behavior of the EMI filter. The first instance of this behavior was observed in the small signal CM IL shown in Fig. 10. Additionally, Fig. 15 shows the shift in the IL curve towards higher frequencies due to an increase in temperature, regardless of the amplitude of the signals applied.

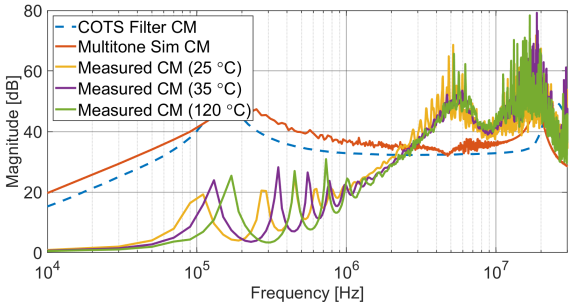

Fig. 15: Effect of a temperature increase in the CM IL for an EMI filter when using a large signal for measurement.

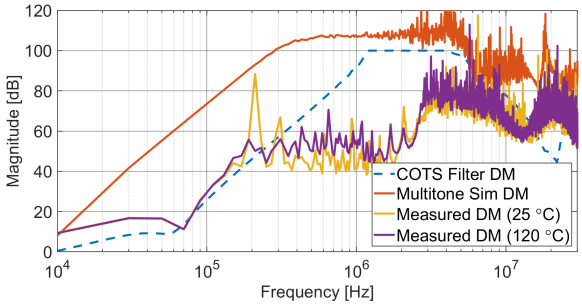

Fig. 16: Effect of a temperature increase in the DM IL for an EMI filter when using a large signal for measurement.

A plausible explanation for the shift to higher frequencies in the IL curve is the change in capacitance of the C_x and

C_y capacitors due to the dielectric dependence on temperature [14] in addition to a change in the permeability of the ferrite core in the CMC, which can lead to an inductance change [28]. Interestingly, the temperature rise only significantly affects the behavior of the CM IL. This is most likely due to the fact that the choke in the EMI filter being measured is a CMC.

The gathered results show that the setup allows the analysis of the NLTV behavior of an EMI filter. The characterization of the filter may be done with a small signal with limited dynamic resolution, or with a large signal which affects the behavior of the EMI filter being measured. Using a large signal to evaluate the filter approximates in-situ performance since the filter is subjected to the voltage and current levels representative of a real world application.

The power levels used affect both CM and DM IL curves. The most notable change occurs in the CM case. Additionally, the results show that an increase in temperature may also change the performance of the filter. This effect, however, only noticeably affects the CM IL and manifests as a change in cut-off frequencies, or a 'shift' down the frequency axis. There is little to no difference in the DM IL due to a temperature change.

VI. Conclusions

Currently, IL measurements of an EMI filter are time-consuming and require multiple measurement setups. These characterization measurements are done in a controlled laboratory setting. Such setup does not allow the study of non-linear filter behavior, or LTV observations.

A setup was developed to evaluate the behavior of an EMI filter simulating in-situ performance. The built setup is able to measure the IL of an EMI filter under high power levels. The accuracy of the measurement depends on a few key parameters: the frequency of the input signal applied, the input signal's magnitude, the rise and fall times of the signal applied, and the resolution of the measurement equipment.

NLTI effects were observed when applying a large input signal. Additionally, LTV effects were observed in the measured IL curves. From the gathered evidence, there is a direct relation between the temperature of the filter and its performance. The notable difference between measuring the filter with a small signal compared to a large signal suggests that the usual EMI filter IL characterization is not representative of in-situ performance. Additionally, the components' surface temperature may change their properties and affect the frequency-domain attenuation.

The setup was well suited to measure the CM and DM IL curves of an EMI filter within a 14.47 MHz bandwidth. Furthermore, the designed setup allows a faster evaluation of an EMI filter by reducing the amount of measurements needed. Finally, the designed setup allows the analysis of NLTV effects on the IL of an EMI filter.

References

[1] Q. Zhaoming, W. Xin, L. Zhengyu, and M. Pong, "Status of electromagnetic compatibility research in power electronics." Int. Acad. Publishers, pp. 46–57.

[2] W.-Y. Chang, Richard, K.-Y. See, W.-S. Soh, Y.-H. Ong, and W. Huang, "Impacts of emi filter on high speed interconnects for digital circuits design," in *2012 Asia-Pacific Symposium on Electromagnetic Compatibility*, 2012, pp. 413–416.

[3] T. Keiler and M. Stadler, "Influence of rf emi filter structures on high speed digital signals," in *2008 6th International Symposium on Communication Systems, Networks and Digital Signal Processing*, 2008, pp. 390–393.

[4] "Methods of measurement of the suppression characteristics of passive emc filtering devices," International Electrotechnical Commission (IEC) Std.

[5] *CISPR17 Measurements*, Schaffner, 3 1996.

[6] D. Nemashkalo, P. Koch, N. Moonen, and F. Leferink, "Multichannel emi filter performance assessment." IEEE, 9 2022, pp. 69–73.

[7] R. Todd, F. Bryan, A. Forsyth, C. Gan, and J. Bossard, "Effects of electrical power off-take on finite inertia mechanical systems." IEEE, 9 2011, pp. 1476–1482.

[8] H. Chen, J. Wu, and X. Zheng, "Elimination of common-mode choke saturation caused by self-resonance of the emi filter in a variable-frequency drive system," *IEEE Transactions on Electromagnetic Compatibility*, vol. 61, no. 4, pp. 1226–1233, 2019.

[9] F. Luo, S. Wang, F. Wang, D. Boroyevich, N. Gazel, Y. Kang, and A. C. Baisden, "Analysis of cm volt-second influence on cm inductor saturation and design for input emi filters in three-phase dc-fed motor drive systems," *IEEE Transactions on Power Electronics*, vol. 25, no. 7, pp. 1905–1914, 2010.

[10] Z. Cong, H. Xu, X. Yang, Z. Zhou, and Y. Cao, "The influence of temperature characteristics and aging of capacitor element on the measurement accuracy of capacitor voltage transformer," in *2020 10th International Conference on Power and Energy Systems (ICPES)*, 2020, pp. 517–521.

[11] C. R. Paul, *Introduction to Electromagnetic Compatibility (EMC)*. John Wiley Sons, Ltd, 2005. [Online]. Available: https://onlinelibrary.wiley.com/doi/abs/10.1002/0471758159.ch1

[12] M. Pous, M. A. Azpurua, D. Zhao, J. Wolf, and F. Silva, "Time-domain multitone impedance measurement system for space applications." IEEE, 9 2022, pp. 247–252.

[13] J. McCloskey, "Effects of rise/fall times on signal spectra," Presentation, NASA.

[14] S. Mao, "Capacitor fundamentals: Part 7 - linear dielectrics," Knowles Capacitors.

[15] C. Chen and X. Xu, "Modeling the conducted emi emission of an electric vehicle (ev) traction drive," in *1998 IEEE EMC Symposium. International Symposium on Electromagnetic Compatibility. Symposium Record (Cat. No.98CH36253)*, vol. 2, 1998, pp. 796–801 vol.2.

[16] O.-H. Gwon, J.-W. Jeon, J. Ahn, H.-S. Kweon, M. ro Kim, S.-Y. Jung, and W. Nah, "Component characteristics of motor drive system in ev/hev and its noise spectrum analysis," in *2013 International Conference on Electrical Machines and Systems (ICEMS)*, 2013, pp. 539–544.

[17] C. R. Paul and K. Hardin, "Diagnosis and reduction of conducted noise emissions," *IEEE Transactions on Electromagnetic Compatibility*, vol. 30, no. 4, pp. 553–560, 1988.

[18] Z. Wang, S. Wang, P. Kong, and F. C. Lee, "Dm emi noise analysis for critical conduction mode pfc," in *2011 Twenty-Sixth Annual IEEE Applied Power Electronics Conference and Exposition (APEC)*, 2011, pp. 1475–1481.

[19] IPC, *IPC-2221 A Generic Standard on Printed Circuit Board Design*, IPC, 2 1998.

[20] J. Kulanayagam, J. Hagmann, S. Schenke, K. Hoffmann, and S. Dickmann, "Numerical modeling for heatsink emissions in power electronics," *Advances in Radio Science*, vol. 10, pp. 239–243, 9 2012.

[21] G. Zhai, W. Yang, and X. Zhou, "Study on conducted emi from operation of electromagnetic relay contacts," in *2008 International Conference on Electrical Machines and Systems*, 2008, pp. 543–547.

[22] *CREE MOSFET Evaluation Kit Manual*, CREE Power, 4 2015, rev. B.

[23] I. Kovacevic, F. Krismer, S. Schroth, and J. W. Kolar, "Practical characterization of emi filters replacing cispr 17 approximate worst case measurements." IEEE, 6 2013, pp. 1–10.

[24] *Silicon Carbide Power MOSFET C2M MOSFET Technology N-Channel Enhancement Mode*, Wolfspeed Inc., 11 2023, rev. B.

[25] N. Baptistat, K. Abouda, G. Duchamp, and T. Dubois, "Impact of asymmetrical shape for trapezoidal signal on ics spectral emission envelope," in *2019 12th International Workshop on the Electromagnetic Compatibility of Integrated Circuits (EMC Compo)*, 2019, pp. 180–182.

[26] *ADC Input Noise: The Good, The Bad, and The Ugly. Is No Noise Good Noise?*, Analog Devices, 2 2006.
[27] W. R. Bennett, "Spectra of quantized signals," in *Bell Systems Technical Journal*, vol. 27, 7 1948, pp. 446–471.
[28] W. Zhang, Q. Yang, Y. Li, Z. Lin, and M. Yang, "Temperature dependence of powder cores magnetic properties for medium-frequency applications," *IEEE Transactions on Magnetics*, vol. 58, no. 2, pp. 1–5, 2022.

APPENDIX

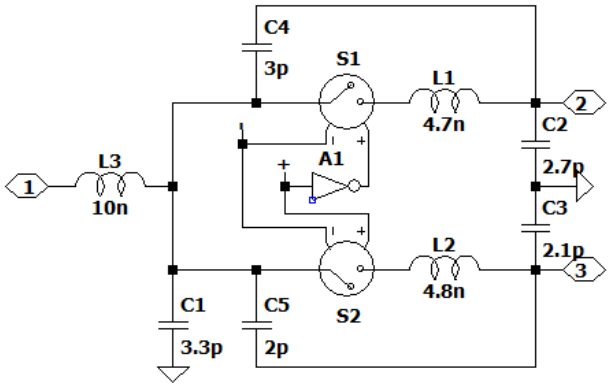

Fig. 17: DPDT switch model (per individual switch).

TABLE II: List of Parameters Used in Model.

Capacitance	**Inductance**	**Resistance**
$C_{x1} = 0.47\,\mu\text{F}$	$ESL\_C_{x1} = 8.6\,\text{nH}$	$ESR\_C_{x1} = 53\,\text{m}\Omega$
$C_{x2} = 0.47\,\mu\text{F}$	$ESL\_C_{x2} = 8.6\,\text{nH}$	$ESR\_C_{x2} = 53\,\text{m}\Omega$
$EPC\_R_1 = 8.9\,\text{pF}$	$ESL\_R_1 = 12\,\text{nH}$	$R_1 = 680\,\text{k}\Omega$
-	$L_{11} = 8\,\text{mH}$	$ESR\_L_{11} = 614\,\text{m}\Omega$
$EPC_{L11} = 37.4\,\text{pF}$	$L\_leak_{11} = 55\,\text{uH}$	$EPR\_L_{11} = 26\,\text{k}\Omega$
-	$L_{12} = 8\,\text{mH}$	$ESR\_L_{12} = 614\,\text{m}\Omega$
$EPC_{L12} = 37.4\,\text{pF}$	$L\_leak_{12} = 55\,\text{uH}$	$EPR\_L_{12} = 26\,\text{k}\Omega$
$C_{W1} = 5\,\text{pF}$	-	-
$C_{W2} = 5\,\text{pF}$	-	-
$C_{y1} = 4.7\,\text{nF}$	$ESL\_C_{y1} = 15\,\text{nH}$	$ESR\_C_{y1} = 120\,\text{m}\Omega$
$C_{y2} = 4.7\,\text{nF}$	$ESL\_C_{y2} = 15\,\text{nH}$	$ESR\_C_{y2} = 120\,\text{m}\Omega$

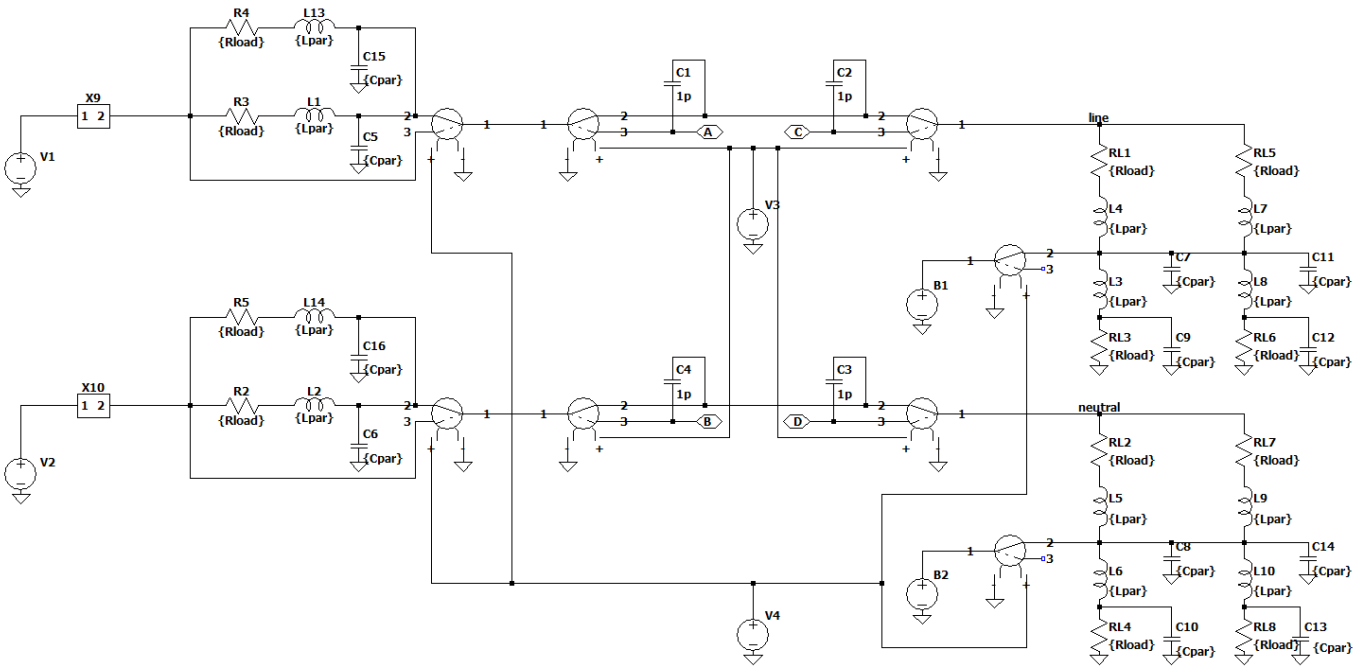

Fig. 18: Modelled setup. $R_{\text{load}} = 100\Omega$, $L_{\text{par}} = 20nH$, $C_{\text{par}} = 13.85pF$, V_1 and V_2 are the driving trapezoidal sources, V_3 controls the unfiltered/filtered configuration, V_4 controls the termination impedance scenario, and B_1 and B_2 are noise sources to simulate the noise in the measurement instruments.

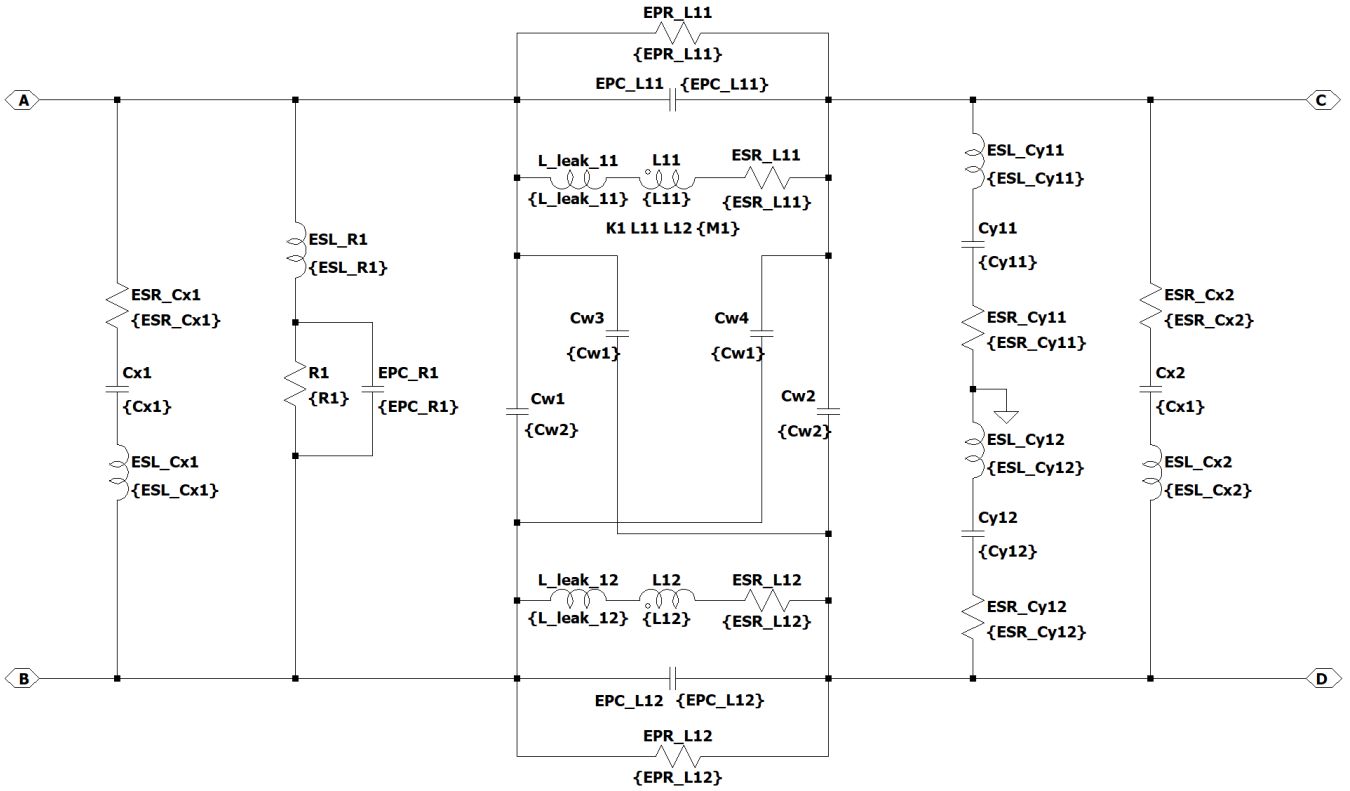

Fig. 19: Equivalent circuit model for the EMI filter being analyzed. The values and parameters used can be found in Table II.